Received: 25 January 2022 | Revised: 22 April 2022 | Accepted: 28 April 2022

DOI: 10.1002/jcc.26893

RESEARCH ARTICLE

Journal of COMPUTATIONAL CHEMISTRY WILEY

Quantum chemical rovibrational analysis of aminoborane and its isotopologues

Moritz Schneider | Guntram Rauhut

Institute for Theoretical Chemistry, University of Stuttgart, Stuttgart, Germany

Correspondence
Guntram Rauhut, Institute for Theoretical Chemistry, University of Stuttgart, Pfaffenwaldring 55, 70569 Stuttgart, Germany.
Email: rauhut@theochem.uni-stuttgart.de

Funding information
Deutsche Forschungsgemeinschaft, Grant/Award Number: Ra656/23-3; Studienstiftung des Deutschen Volkes

Abstract

Aminoborane, H_2NBH_2 and its isotopologues, $H_2N^{10}BH_2$, D_2NBD_2, and $D_2N^{10}BD_2$, have been studied by high-level ab initio methods. All calculations rely on multi-dimensional potential energy surfaces and dipole moment surfaces including high-order mode coupling terms, which have been obtained from electronic structure calculations at the level of explicitly correlated coupled-cluster theory, CCSD(T)-F12, or the distinguishable cluster approximation, DCSD. Subsequent vibrational structure calculations based on second-order vibrational perturbation theory, VPT2, and vibrational configuration interaction theory, VCI, were used to determine rotational constants, centrifugal distortion constants, vibrationally averaged geometrical parameters and (an)harmonic vibrational frequencies. The impact of core-correlation effects is discussed in detail. Rovibrational VCI calculations were used to simulate the gas phase spectra of these species and an in-depth analysis of the ν_7 band of aminoborane is provided. Color-coding is used to reveal the identity of the individual progressions of the rovibrational transitions for this particular mode.

KEYWORDS
aminoborane, rovibrational calculations, vibrational configuration interaction theory

1 | INTRODUCTION

While ethylene serves as a benchmark molecule for computational rovibrational studies,[1–3] little has been done for the isoelectronic aminoborane, H_2NBH_2, also termed aminoborane(2) or boranamine. Several studies exist, in which its structural parameters and the harmonic frequencies have been determined, but anharmonic investigations and rovibrational studies are still missing.[4,5] This is surprising as the rovibrational infrared (IR) spectrum is fairly complex and challenging. In 1985, Gerry et al.[6] measured the IR spectrum of aminoborane in the gas phase for the first time. It is dominated by strong overlapping rotational sidebands, which renders its analysis tedious. As the assignment of the vibrational modes by these authors was incomplete and included only estimates of some fundamentals Carpenter and Ault[7] performed matrix isolation measurements in argon and nitrogen matrices. However, the gas phase and matrix isolation results partly differ substantially indicating nonnegligible cage effects (see the NIST database[8] for a direct comparison). Sugie et al.[9] measured the microwave spectrum of H_2NBH_2 and thus provided geometrical parameters and rotational constants being deduced from these spectra. Four years later, Vormann et al.[10] reinvestigated the microwave spectrum and provided all spectroscopic constants as occurring in Watson's A and S reduced Hamiltonians.[11–13] These experimental works serve as reference data within this computational study.

On the other hand, due to its limited size and its C_{2v} symmetry, aminoborane has repeatedly been subject of quantum chemical studies based on density functional theory, Møller–Plesset perturbation theory or, most accurately, on coupled-cluster calculations.[4,5,14] The most comprehensive works in that direction have been provided by Dixon and Gutowski[4] in the context of hydrogen storage as well as

Richard and Ball.[5] Most of the computational studies focus on structural parameters, harmonic vibrational frequencies, proton affinities, the enthalpy of formation, etc., while to the best of our knowledge in-depth spectroscopy studies have not yet been performed. However, due to the enormous increase of compute power and the development of new methods within the recent past, vibrational structure calculations beyond the harmonic approximation[15] are applicable nowadays for systems of up to 20 atoms,[16] if very high accuracy is needed. The workhorse in that direction is second-order vibrational perturbation theory (VPT2),[17,18] which is based on a quartic force field (QFF)[19] and is thus restricted to semi-rigid molecules. Contrarily, vibrational configuration interaction (VCI) theory[20–23] or vibrational coupled-cluster (VCC) theory[24,25] are usually based on arbitrary potential energy surfaces (PES) and are in principle unlimited in accuracy. Clearly, such calculations go along with higher computational demands, but newly developed techniques allow for an efficient and automated calculation of highly accurate spectra.[22,23,26] Quite recently, rovibrational line intensities for IR[27] and Raman spectra[28] have been implemented into the Molpro package of ab initio programs,[29] which allow for the convenient simulation of high-resolution gas phase spectra.

In this work, we provide anharmonic calculations employing vibrational configuration interaction (VCI) theory relying on high-level potential energy surfaces. Moreover, rovibrational calculations have been performed to simulate and analyze the gas phase IR spectra of aminoborane and three isotopologues of it.

2 | COMPUTATIONAL DETAILS

The equilibrium structures of aminoborane and its isotopologues have been determined by explicitly correlated coupled-cluster calculations in combination with a basis set of triple-ζ quality, that is, CCSD(T)-F12b/cc-pVTZ-F12.[30] The aug-cc-pVTZ/MP2FIT basis set of Weigend et al.[31] was used as auxiliary basis. For evaluating the Fock matrix the cc-pVTZ/JKFIT basis set[31] was used. The complementary auxiliary basis set (CABS) approach was employed, i.e. the union of the atomic orbital and the RI basis sets was used to approximate the resolution of the identity (RI). The Hartree–Fock energies were corrected by addition of the CABS singles correction. Normal mode analyses were performed at the same level of theory. The resulting normal coordinates were used to span a multidimensional potential energy surface (PES) represented by an n-mode expansion being truncated after the four-mode coupling terms.[32,33] A multilevel scheme[26,34] has been employed to limit the computational effort for the generation of the PES, that is, the one-mode and two-mode coupling terms have been evaluated at the CCSD(T)-F12b/cc-pVTZ level, while the three-mode and four-mode couplings were determined by the explicitly correlated distinguishable cluster approximation and a double-ζ basis set, DCSD-F12b/cc-pVDZ-F12.[35,36] This multilevel scheme led to significant CPU time savings, while retaining the high accuracy of the PES. Likewise, a multilevel n-mode representation of the dipole moment surface has been determined at the DCSD/cc-pVTZ-F12 (1D and 2D) and DCSD/cc-pVDZ-F12 (3D and 4D) levels. Note that, the distinguishable cluster approximation yields results close to CCSD(T) quality without an explicit evaluation of triple-excitations. In total, 140,719 single point calculations were needed to yield converged results within this representation of the PES and DMS. This corresponds to 4–6 ab initio calculations per dimension. The C_{2v} symmetry of the molecules has been exploited within the electronic structure calculations and the individual mode coupling terms (subsurfaces).[37] On a customary workstation with two Intel Xeon E5-2650 v4 processors representing a total of 24 cores @ 2.10 GHz and 512 GB of global memory, these calculations took no longer than 42 h. The grid representations of these surfaces were transformed to an analytical (polynomial) one using efficient Kronecker product fitting.[38] Not more than seven monomials were needed per dimension. Besides these calculations utilizing the frozen core approximation, an additional set of calculations has been performed including core-correlation effects. In order to describe the molecular orbital basis properly, basis functions including tight core functions have been used in these calculatons, i.e. cc-pcVTZ-F12 etc.[39] Different exponents γ were used for the Slater geminal functions referring to core–core, core–valence, and valence–valence orbital pairs, that is, 0.8, 1.7, and 2.2, as recommended by Werner et al.,[40] while for the frozen calculations a constant γ of 1.0 has been chosen.

Subsequent vibrational self-consistent field (VSCF) calculations relying on a local basis of 18 distributed Gaussians were used to optimize state-specific one-mode wave functions (modals). These were employed in symmetry adapted configuration-selective vibrational configuration interaction (VCI) calculations.[22,23,41] The initial correlation space included up to six-tuple excitations and was restricted by a maximum excitation level of 7 and the sum of quantum numbers not being larger than 15. This resulted in 1.5×10^6 (A_2, B_2) and 1.7×10^6 (A_1, B_1) configurations (Hartree products) in dependence on the irreducible representation of the state of interest. A constant μ-tensor, as occurring in the Watson Hamiltonian for polyatomic molecules,[42] was used within the calculations of the vibrational angular momentum terms for the vibrational states ($J = 0$). The impact of higher order terms of the μ-tensor expansion was found to be negligible. About 60 (H_2NBH_2) to 75 ($D_2N^{10}BD_2$) low lying VCI states were employed in the subsequent rovibrational calculations. The maximal rotational quantum number J_{max} was set to 50 in all calculations. A molecule-specific rotational basis (MSRB) obtained from a primitive rigid rotor basis with modified Wang combinations[43,44] was used within all calculations.[27] This leads to a reliable state assignment in the calculations of rovibrational energies and wave functions, especially in spectral regions with strong Coriolis coupling. A constant μ-tensor was employed within the Coriolis coupling terms, while the rotational kinetic energy contributions also included first- and second-order terms of the n-mode expansion of the μ-tensor. In contrast to the IR intensities for the $J = 0$ calculations, which are based on the assumption of zero temperature, rovibrational line intensities were determined at a temperature of 300 K and nuclear spin statistical weights were obtained from the Landau-Lifshitz formula corrected by Jonas.[45]

TABLE 1 Geometrical parameters of aminoborane and its isotopologues

			VCI/$H_2N^{11}BH_2$		VCI/$H_2N^{10}BH_2$		VCI/$D_2N^{11}BH_2$		VCI/$D_2N^{10}BD_2$	
Parameter	$r_e^{(fc),a}$	$r_e^{(ae),b}$	r_a	r_g	r_a	r_g	r_a	r_g	r_a	r_g
r(NB)	1.3909	1.3870	1.3991	1.3999	1.3992	1.4001	1.3979	1.3992	1.3980	1.3994
r(NH)	1.0047	1.0036	1.0061	1.0239	1.0062	1.0239	1.0062	1.0188	1.0062	1.0188
r(BH)	1.1939	1.1905	1.2031	1.2155	1.2032	1.2155	1.2007	2.2094	1.2008	1.2096
∠(HNB)	123.13	123.11	122.88		122.88		122.97		122.97	
∠(HBN)	118.80	118.83	118.90		118.90		118.87		118.87	

[a]CCSD(T)-F12b/cc-pVTZ-F12 equilibrium geometry within the frozen core approximation.
[b]CCSD(T)-F12b/cc-pcVTZ-F12 equilibrium geometry including core correlation effects.

A detailed discussion concerning the calculation of rovibrational line intensities within the VSCF/VCI formalism is given in reference 27. In addition so-called RCI calculations[27] have been performed, in which rovibrational interactions between different vibrational states are entirely neglected. As each RCI-matrix is constructed for an individual VCI wave function, the vibrational state identity can be trivially assigned for every rovibrational state. Contrarily, within RVCI calculations all rovibrational interactions are considered. As a consequence the only" good" quantum number is the angular momentum quantum number *J* and the parity of the rovibrational state, while the assignment to vibrational states may be error-prone. According to this, RVCI provides physically meaningful results, while RCI does not. However, a comparison of the spectra obtained from these methods is helpful within the interpretation of the spectra and the discussion of rovibrational couplings. Moreover, VPT2 relying on a quartic force-field being retrieved from the polynomial representation of the *n*-mode expansion of the PES has been used to determine vibrational frequencies, IR intensities, vibrationally averaged rotational constants and equilibrium centrifugal distortion constants.[13,17,19] All calculations have been performed with the Molpro package of ab initio methods[29] and the molecules were oriented according to the I^r convention in all cases.

3 | RESULTS AND DISCUSSION

3.1 | Geometrical parameters and spectroscopic constants

The structural parameters corresponding to the minimum of the PES, r_e, and the parameters obtained from vibrational averaging are listed in Table 1. All values refer to calculations utilizing the frozen core approximation except the data for the equilibrium structure as provided in the third column of the table. While the r_a parameters were obtained from the atomic positions averaged over the VCI ground state wavefunction, the r_g parameters are instantaneous internuclear distances calculated from an expectation value of the bond lengths expanded in terms of the normal coordinates. Sugie et al.[9] determined r_s structural parameters for H_2NBH_2 from the microwave spectra of five isotopic species of aminoborane to be r_s (NB) = 1.391(2) Å, r_s (NH) = 1.004(2) Å, r_s (BH) = 1.195(4) Å, ∠ (HNB) = 122.9(2)° and ∠ (HBN) = 118.9(2)°. Although these values cannot directly be compared, the agreement of these experimental r_s values with our computed $r_e^{(fc)}$ values is excellent. Moreover, r_e values have been computed by several authors using different levels of electronic structure theory, see for example the compilation of data in the paper of Richard and Ball.[5] With respect to their calculations at the G2, G3 level of theory, we obtain slightly longer hydrogen bond lengths. As must be expected, due to anharmonic effects vibrational averaging leads to an elongation of all bonds, while the bond angles are hardly affected. Contrarily, core correlation effects lead to slightly shorter bond lengths, which in turn will lead to somewhat larger rotational constants (see the following text).

As the polynomial representation of the PES allows for a determination of the spectroscopic constants of Watson's A and S reduced Hamiltonians[11–13] based on VPT2,[13,17] the corresponding values are summarized in Table 2.

According to the rotational constants aminoborane is an asymmetric top molecule tending towards a near prolate symmetric top. This character is less pronounced for deuterated species, for which the A rotational constant is much smaller. In comparison to the experimental data of Vormann et al.[10] and those of Sugie et al.[9] for $H_2N^{11}BH_2$ our computed VPT2-based spectroscopic constants obtained from PESs relying on frozen core electron correlation methods tend to underestimate the experimental values. However, a substantial improvement can be obtained by including core-correlation effects. While the largest deviation of the computed rotational constants from the results of Vormann et al.[10] is 0.52% for the frozen-core calculations, it is just 0.036% when accounting for these additional contributions. For that reason, the spectroscopic constants determined for the isotopologues refer to core-correlation calculations only (see Table S1, Supporting Information, for the frozen core results). However, it is well known that accounting for core-correlation effects alone usually leads to slightly unbalanced calculations, because high-level electron correlation contributions as arising for example from CCSDT(Q) calculations, which were out of range within this study, tend to cancel these effects.[46–48] Therefore, the excellent agreement of our computed rotational constants with the experimental reference data most likely relies to some extent on error cancellation. For that reason, in the following, we will provide mainly

TABLE 2 VPT2 spectroscopic constants of aminoborane and its isotopologues

		$H_2N^{11}BH_2$					
	Unit	Exp.[a]	Calc.(ae)[b]	Calc.(fc)[c]	$H_2N^{10}BH_2$	$D_2N^{11}BD_2$	$D_2N^{10}BD_2$
A_e	GHz		139.73346	139.22625	139.73346	69.92044	69.92044
B_e	GHz		27.71535	27.57358	28.65986	20.54797	21.04659
C_e	GHz		23.12804	23.01541	23.78207	15.88094	16.17714
S Reduction							
A	GHz	138.22139(9)	138.27109	137.76695	138.26370	69.38757	69.37506
B	GHz	27.487267(2)	27.48736	27.34581	28.41991	20.41046	20.90401
C	GHz	22.878827(3)	22.87804	22.76763	23.52167	15.73822	16.02960
D_J	kHz	43.07(3)	42.949	42.694	45.631	22.320	23.603
D_{JK}	kHz	314.6(3)	312.477	310.773	320.002	100.588	99.356
D_K	MHz	2.58(2)	2.465	2.450	2.455	0.58425	0.58411
d_1	kHz	−8.615(3)	−8.417	−8.352	−9.271	−6.512	−7.044
d_2	kHz	−1.565(3)	−1.460	−1.447	−1.634	−1.334	−1.438
A Reduction							
A	GHz	138.22138(9)	138.27109	137.76695	138.26370	69.38757	69.37506
B	GHz	27.487889(3)	27.48736	27.34581	28.41991	20.41046	20.90401
C	GHz	22.878220(3)	22.87804	22.76763	23.52167	15.73822	16.02960
Δ_J	kHz	46.22(3)	45.869	45.587	48.900	24.987	26.480
Δ_{JK}	kHZ	295.8(3)	294.958	293.414	300.392	84.585	82.098
Δ_K	MHz	2.59(2)	2.479	2.464	2.471	0.59759	0.59849
δ_J	kHz	8.621(3)	8.417	8.352	9.271	6.512	7.044
δ_K	kHz	307.2(6)	291.037	289.262	304.236	118.199	121.237

[a]Taken from Reference 10.
[b]All electron PES includes core-correlation effects.
[c]PES calculated within the frozen core approximation.

results from frozen-core calculations, but respective results corresponding to all electron calculations can be found in the supplementary material.

3.2 | Vibrational frequencies

Table 3 shows the computed fundamental transitions, harmonic values and anharmonic VPT2 and VCI results, and IR intensities for H_2NBH_2 in comparison to experimental data taken from the literature.[6–8] A visualization of the vibrational modes within the harmonic approximation is provided in Figures S3–S6, Supporting Information. We note here that the character of the individual vibrations, as provided in Table 3 does not change for the other isotopologues. The overall agreement of our VCI results with the experimental values is excellent and a number of tentative misassignments in the experimental works of Gerry et al.[6] and Carpenter and Ault[7] simply reveal the difficulties associated with this molecule. We will discuss these cases in detail below. Moreover, except for ν_8 the VPT2 results agree very well with the more accurate VCI results, which must be expected for this fairly rigid molecule. The vibrational states 2^1 and 3^1 are strongly affected by resonances. For ν_2 it is a type II Fermi resonance with the combination band $\nu_4 + \nu_5$ at 2455.1 cm^{-1} which leads to strong couplings and a low leading VCI coefficient of 0.74 (55%). For ν_3, it is an even stronger type II Fermi resonance with the combination band $\nu_7 + \nu_8$ and an admixture of the $2\nu_6$ overtone. We observe two transitions, the first one at 1602.0 cm^{-1}, the other one at 1618.6 cm^{-1}. The coupling between these states is so strong, that it is hardly possible to pinpoint the fundamental, which has lost its identity. Formally, the fundamental should be the one at 1602.0 cm^{-1} (44%), but as the other one shows much better agreement with the experimental assignment, we followed the decision of the experimentalists, that is, 1618.6 cm^{-1}, which is equally good. As these transitions have fairly strong IR intensities, the spectrum of aminoborane shows a number of overtones and combination bands, which contribute to the spectrum (see Tables S2–S9, Supporting Information).

Moreover, in their first data compilation, Gerry et al.[6] assigned the transition ν_6, ν_8, and ν_{12} on the basis of perturbations in ν_4. According to our calculations and the reassignment of Gerry and coworkers (last column in Table 3), the original assignment is not reliable, while the reassigned values are in good agreement with our VCI results. Moreover, Gerry et al.[6] assigned a band at 1225 cm^{-1} to be the mode ν_5. This is in contradiction to our calculations and the results of Carpenter and Ault.[7] Most likely, this band belongs to the overtone

TABLE 3 Computed fundamental wavenumbers [cm^{-1}] and IR intensities [km/Mol] for $H_2N^{11}BH_2$

Sym.	#	Harm.	VPT2	IR(VPT2)[a]	VCI	IR(VCI)[a]	Exp.[b]	Exp.[c]	Exp.[d]	Description
A_1	ν_1	3607.2	3453.6	18.9	3450.6	18.3	3437	3451		NH stretch
	ν_2	2586.2	2490.9	49.8	2491.1[e]	58.1	2499	2495		BH stretch
	ν_3	1653.2	1610.1	44.1	1618.6[e]	17.1	1620	1625		NH_2 scissors
	ν_4	1364.1	1328.3	70.1	1334.0	76.5	1334	1337		BN stretch
	ν_5	1160.3	1140.4	0.6	1140.0	2.2	1120	1225[f]		BH_2 scissors
A_2	ν_6	861.0	824.0	0.0	827.5	0.0		(763)[g]	820	Torsion
B_1	ν_7	1016.6	997.1	26.7	1003.2	25.4	1002	1005		NH_2 wag
	ν_8	611.0	563.0	179.6	604.5	165.1	705	(670)[g]	612	BH_2 wag
B_2	ν_9	3707.7	3525.2	24.4	3532.5	21.8	3519	3534		NH stretch
	ν_{10}	2666.4	2558.4	131.0	2558.4	156.8	2568	2564		BH stretch
	ν_{11}	1143.4	1115.3	35.1	1118.1	35.4	1022	1131[f]		NH_2 rock
	ν_{12}	741.1	733.5	0.7	736.3	0.5	608	(595)[g]	742	BH_2 rock

[a]IR intensity in dependence of the method.
[b]Ar matrix isolation data, taken from reference 7.
[c]Gas phase data, taken from reference 6.
[d]Taken from the NIST database.[8]
[e]Strong Fermi resonance, see the discussion section.
[f]Tentative misassignment, see the discussion section.
[g]Estimated from perturbations in ν_4.

TABLE 4 Computed fundamental frequencies (cm^{-1}) and IR intensities (km/mol) for $H_2N^{10}BH_2$, $D_2N^{11}BD_2$, and $D_2N^{10}BD_2$

		$H_2N^{10}BH_2$			$D_2N^{11}BD_2$			$D_2N^{10}BD_2$		
Sym.	#	Harm.	VCI	IR	Harm.	VCI	IR	Harm.	VCI	IR
A_1	ν_1	3607.2	3451.5	18.6	2611.5	2524.7	17.0	2611.8	2528.5	17.8
	ν_2	2592.8	2474.1	72.8	1889.8	1836.4	81.5	1905.0	1851.2	87.5
	ν_3	1655.7	1607.5	46.5	1371.9	1343.5	87.8	1391.3	1361.8	87.2
	ν_4	1396.3	1364.7	75.0	1123.3	1107.5	3.2	1134.5	1118.0	1.5
	ν_5	1163.3	1142.9	1.3	857.6	846.4	1.8	857.6	846.2	1.8
A_2	ν_6	861.0	827.4	0.0	609.0	591.9	0.0	609.0	591.8	0.0
B_1	ν_7	1029.6	1015.7	26.1	811.2	802.5	21.5	827.5	818.5	22.1
	ν_8	611.4	604.8	164.5	474.8	469.3	88.8	474.9	469.3	88.6
B_2	ν_9	3707.7	3532.4	21.7	2738.5	2641.8	14.7	2738.5	2641.9	14.6
	ν_{10}	2682.6	2575.3	153.5	2002.1	1936.7	95.7	2025.2	1958.4	98.7
	ν_{11}	1153.5	1127.7	35.0	925.2	910.6	14.6	934.3	919.5	14.2
	ν_{12}	741.9	736.9	0.5	532.5	530.5	0.2	533.3	531.2	0.2

$2\nu_8$, which we computed at 1222.4 cm^{-1} and which shows an IR intensity of 18.4 km/mol. As a consequence of this misassignment, Gerry et al.[6] correlated the band at 1131 cm^{-1} with ν_{11}, which should be ν_5. Based on these assignments, the mean absolute deviation (MAD) for the fundamental transition (except for ν_{11}, for which no reliable experimental data are available) of our VCI calculations is 4.8 cm^{-1}. This value is slightly larger than those for other comparable molecules, but still must be considered an excellent result. Accidentally, the VCI results obtained from a PES including core-correlation effects yields exactly the same MAD, but of course the deviations for the individual transitions differ from the frozen core calculations (see Tables S2–S9, Supporting Information).

TABLE 5 Nuclear spin statistical weights for aminoborane and its isotopologues

Sym.	$H_2N^{11}BH_2$	$H_2N^{10}BH_2$	$D_2N^{11}BD_2$	$D_2N^{10}BD_2$
A	120	210	540	945
B	72	126	432	756

The results for the other isotopologues, for which no experimental data are available, are presented in Table 4. $H_2N^{10}BH_2$ shows the same Fermi resonances as $H_2N^{10}BH_2$, but of course the ratios are slightly shifted and the assignment in general is more reliable. For the

deuterated species, resonances play a minor role for the fundamental modes.

3.3 | Rovibrational calculations

Rovibrational spectra have been computed in an automated fashion as described in detail in reference 27. An important quantity, which enters into the equation for the line strength of the state of interest in dependence on its irrep is the nuclear spin statistical weight (NSSW). The NSSWs for aminoborane and its isotopologues are listed in Table 5. Note that the ratios, that is, NSSW(A)/NSSW(B), are identical for $H_2N^{11}BH_2$ and $H_2N^{10}BH_2$ and also for the pair of the deuterated molecules, but differ substantially with respect to their absolute values. However, the latter aspect is of minor importance for the appearance of the spectra as we will consider relative intensities, that is the spectra are scaled with respect to the intensity of a well-defined state (see the following text).

In a first step, we have simulated the rovibrational IR spectra at a temperature of 300 K. In order to account for line broadening effects a Gaussian profile with a half-width (FWHM) of 0.5 cm^{-1} has been applied to the line list. For a better comparison of the spectra for the different isotopologues, they were normalized with respect to the peak of the pure rotational band. The corresponding plots are shown

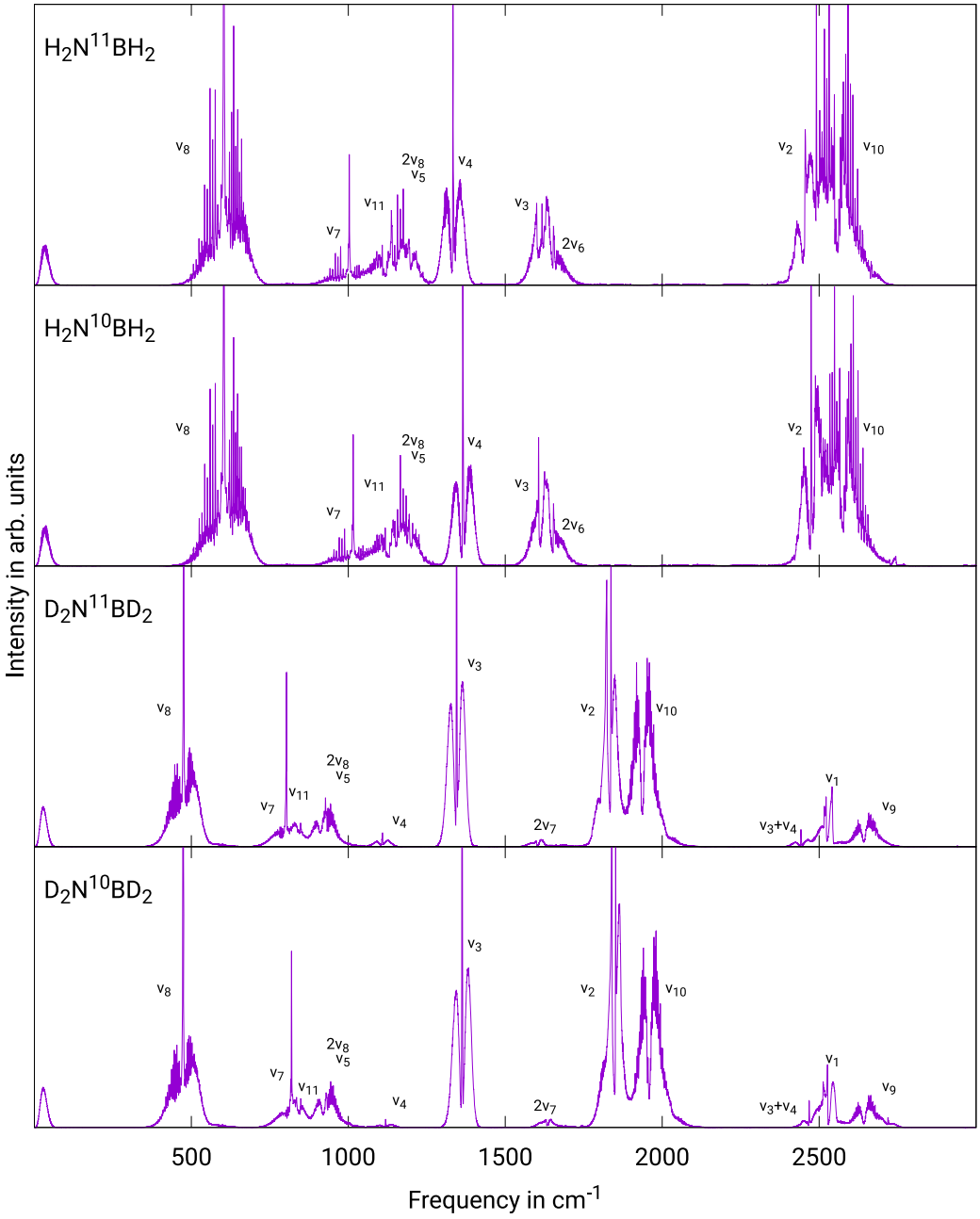

FIGURE 1 Rovibrational infrared (IR) spectra of aminoborane and three of its isotopologues. All spectra are adjusted with respect to the maximum of the peak of the pure rotational band (far left). A Gaussian profile with a half-width (FWHM) of 0.5 cm^{-1} has been applied in all cases.

in Figure 1. In principle the simulated spectrum of aminoborane (uppermost plot in Figure 1) can be compared with the low-resolution transmittance spectrum of Gerry et al.[6] However, a direct comparison is difficult and questionable, because the error bar in our PES is still too large to allow for that. Moreover, a simple Gaussian line-broadening can hardly represent the experimental conditions and the experimental spectrum also contains impurities etc. Therefore, we refrain from showing a direct comparison, but want to emphasize that the similarity of our simulation with the experimental spectrum is apparent, that is, the strong band around 2500 cm^{-1} qualitatively shows the same appearance as in our simulation and likewise do the peaks at about 1335 and 1625 cm^{-1}. In the range of 900 cm^{-1} to 1250 cm^{-1} a complex feature arising from different modes is observed as well. A comparison of the rovibrational spectra for the different molecules reveals that the change from the ^{11}B isotope to the ^{10}B isotope only leads to a modest alteration of the overall appearance of the spectra. Contrarily, as must be expected the impact upon deuteration is tremendous. Beside the shift of the frequencies, significant changes in the intensities can be observed. This can be seen for the hardly shifted bands at about 1350 cm^{-1}, that is, ν_4 for the nondeuterated systems and ν_3 for the deuterated molecules. Also the strongly coupled feature between 900 and 1250 cm^{-1}, which has been shifted to 700–1000 cm^{-1} shows a different relative intensity. But not only the intensity, but also the appearance of the individual peaks changes, for example, the broad feature at 2400–2700 cm^{-1} (nondeuterated species) corresponding to the ν_2 and ν_{10} transitions, which is shifted to 1800–2050 cm^{-1} (deuterated species), splits up in two less coupled patterns. This underlines the sensitivity of these spectra.

As mentioned above, the region between 900 and 1250 cm^{-1} shows a complex pattern arising from the interaction of several bands. In order to analyze this specific part of the spectrum in more detail, we switched to a high-resolution representation, that is, a bar plot, neglecting any effects arising from line-broadening. Figure 2 shows the RCI and RVCI spectra of H_2NBH_2 (the corresponding all electron plot is shown in Figure S1, Supporting Information). Within this plot, we have assigned the individual rovibrational bands by color to the four contributing vibrational states 5^1, 7^1, 11^1, and 8^2. As the vibrational quantum number is not a good quantum number, the assignment with respect to vibrational state will be error-prone once the leading coefficient becomes very low. This is a well-known problem, which arises from the color-coding, but has no impact on the existence and strength of the individual lines. Such problems can bee seen for the transitions assigned to ν_5 in the low-frequency region, but these are irrelevant for an interpretation of the spectrum. Besides that, most progressions and branches are securely assigned. As can be seen, the transitions belonging to ν_5 and $2\nu_8$ are almost completely hidden by dominating rotational sidebands of ν_{11}. In other words: if the spectrum would have been plotted solely in black it would have been a tedious task to decide which line belongs to which vibration. Comparing the RCI with the RVCI spectra reveals the influence of the rovibrational coupling. For example, the R branch of the fundamental ν_{11} is not only broader, but also more intense in the RVCI spectrum. Additionally, mode ν_5 is also more intense in the RVCI spectrum, indicating strong couplings with ν_{11}. Contrarily, the transitions for ν_7 and $2\nu_8$ are significantly less affected by rovibrational couplings as the RCI and RVCI spectra are very similar.

Moreover, color-coding can also be used to reveal further details of the spectrum. For that very reason, we isolated the transitions assigned to ν_7 in the region between 850 and 1100 cm^{-1} (this corresponds to the brownish transitions in Figure 2). In this new plot

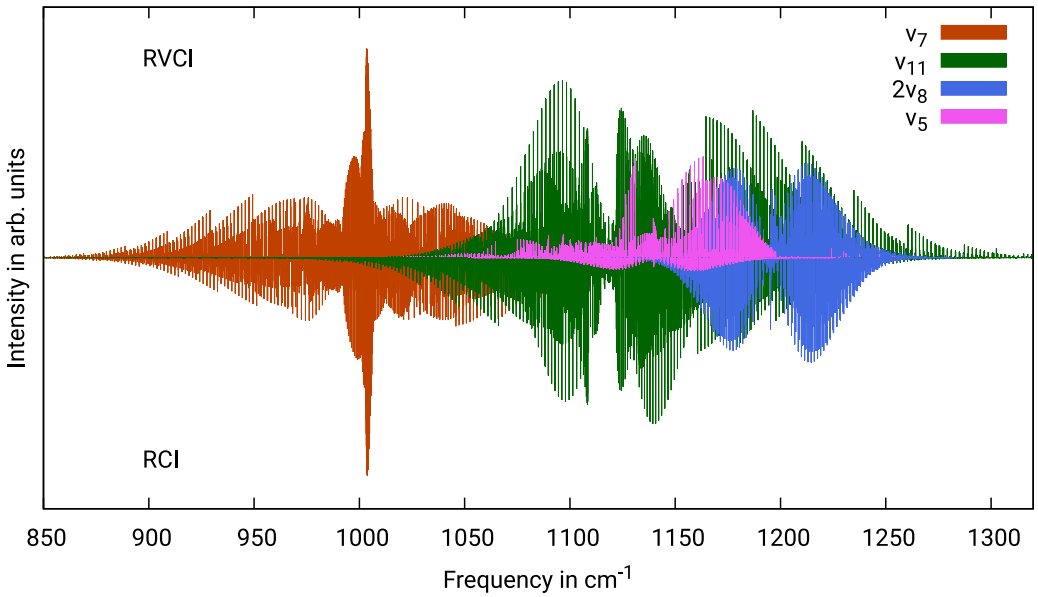

FIGURE 2 Ab initio rovibrational IR spectrum of H_2NBH_2 in the range of 850 cm^{-1} to 1300 cm^{-1}. RVCI and RCI calculations reveal the impact of rovibrational couplings.

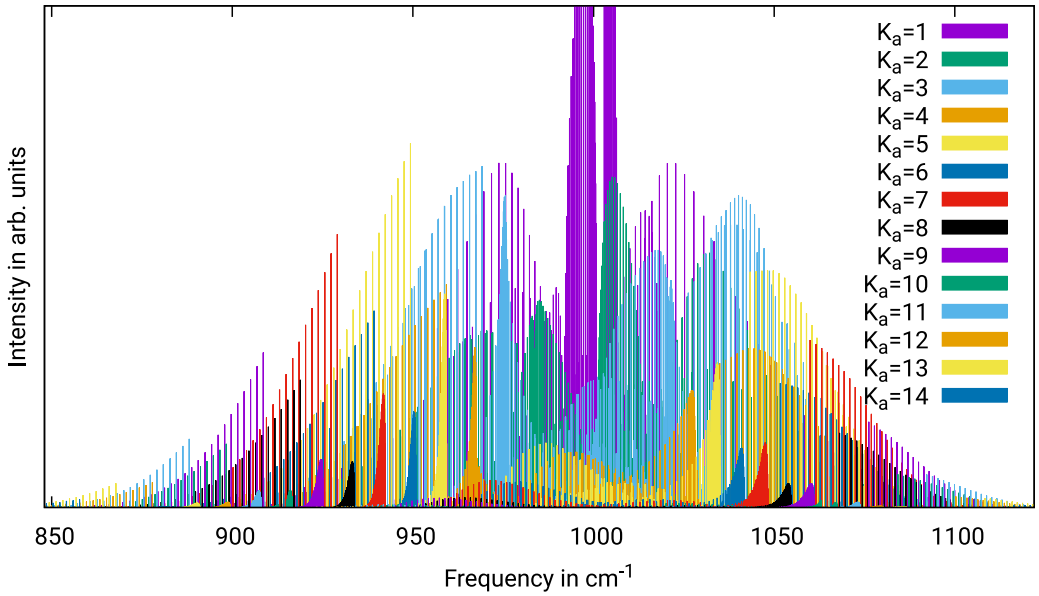

FIGURE 3 Rovibrational IR spectrum of the ν_7 mode. Color-coded are the transitions with respect to the K_a quantum number of the excited state. Plotted are the transitions up to $K_a = 14$.

(cf. Figures 3 and S2, Supporting Information), we have used different colors with respect to the assigned K_a quantum number. This coding allows to distinguish between the different subbands of this mode. Of particular interest are the types of the encoded subbands. In the spectrum, bands with little intensity are spread over the whole range and can be identified as Q branches. It is well-known that widely distributed Q branches represent a perpendicular band, in the case of an asymmetric nearly prolate rotor, a B- or C-type band.[49] Another feature observed in the spectrum is the really strong Q branch in the center of the band. This leads to the assumption of a parallel band, or rather a A-type band in this asymmetric case.[49] Both observations can be consolidated by comparison with the dipole moments associated with this particular mode. The mode describes an out of plane movement of the molecule, which leads to an change of the dipole moment along the *a* and the *c* axes. Those two axes represent a parallel and a perpendicular axis, respectively, and thus confirm the observations seen in the spectrum. Besides that, due to the color-coding the individual progressions in this plot can now easily be assigned to the K_a quantum number of the excited state. Note that contributions assigned to odd K_a values are stronger than those for even values and dominate the overall appearance of this band.

4 | SUMMARY AND CONCLUSIONS

High-level rovibrational calculations based on a multidimensional potential energy and dipole moments surfaces obtained from explicitly correlated coupled-cluster calculations and the distinguishable cluster approximation were used to study the gas phase spectra of aminoborane and three of its isotopologues. The inclusion of core-correlation effects within the electronic structure calculations resulted in rotational constants being in much better agreement with experimental reference data than those obtained from comparable calculations employing the frozen core approximation. The computed vibrational spectra, which show strong Fermi resonances for some of the modes, are in excellent agreement with experimental results with an MAD as low as 4.8 cm^{-1}. A high-level estimate for one yet unassigned fundamental mode is provided for aminoborane and all fundamental modes of the isotopologues. A detailed analysis of the rovibrational spectrum of aminoborane has been provided for the spectral region between 900 and 1300 cm^{-1}. Four strongly coupling modes, ν_5, ν_7, ν_{11}, and $2\nu_8$, contribute to this part of the spectrum. Color-coding with respect to the vibrational and K_a quantum numbers for the rovibrational transitions of aminoborane provides insight with respect to the contributing progressions for the first time. Consequently, these calculations reveal details of the vibrational structure of aminoborane and thus allow for a better understanding of the experimental results. All calculations have been performed with a new and highly automated program within the Molpro package of ab initio programs and can efficiently be controlled by a few keywords only.

ACKNOWLEDGMENTS

The authors are grateful for insightful discussions with M. Tschöpe and Dr. B. Schröder. Financial support by the Deutsche Forschungsgemeinschaft (project Ra656/23-3) and the Studienstiftung des Deutschen Volkes is kindly acknowledged. Open Access funding enabled and organized by Projekt DEAL.

DATA AVAILABILITY STATEMENT

The data that support the findings of this study are available from the corresponding author upon reasonable request. The potential

energy surfaces for aminoborane and its isotopologues can be downloaded from the Zenodo database (https://doi.org/10.5281/zenodo.6475421).

ORCID

Guntram Rauhut https://orcid.org/0000-0003-0623-3254

REFERENCES

[1] B. P. Mant, A. Yachmenev, J. Tennyson, S. N. Yurchenko, *Mon. Not. R. Astron. Soc.* **2018**, *478*, 3220.
[2] S. Carter, A. R. Sharma, J. M. Bowman, *J. Chem. Phys.* **2012**, *137*, 154301.
[3] G. Avila, T. Carrington Jr., *J. Chem. Phys.* **2011**, *135*, 064101.
[4] D. A. Dixon, M. Gutowski, *J. Phys. Chem. A* **2005**, *109*(23), 5129.
[5] R. M. Richard, D. W. Ball, *THEOCHEM J. Mol. Struct.* **2007**, *823*, 6.
[6] M. C. L. Gerry, W. Lewis-Bevan, A. J. Merer, N. P. C. Westwood, *J. Mol. Spectrosc.* **1985**, *110*, 153.
[7] J. D. Carpenter, B. S. Ault, *J. Phys. Chem.* **1991**, *95*, 3502.
[8] NIST Chemistry WebBook, NIST Standard Reference Database Number *69*, P.J. Linstrom and W.G. Mallard, National Institute of Standards and Technology, Gaithersburg MD, 20899, (accessed: January 20, 2022, https://doi.org/10.18434/T4D303.
[9] M. Sugie, H. Takeo, C. Matsumura, *J. Mol. Spectrosc.* **1987**, *123*, 286.
[10] K. Vormann, H. Dreizler, J. Doose, A. Guarnieri, *Z. Naturforsch.* **1991**, *46a*, 770.
[11] J. K. G. Watson, *J. Chem. Phys.* **1967**, *46*(5), 1935.
[12] J. K. Watson, Aspects of quartic and sextic centrifugal effects on rotational energy levels. in *Vibrational spectra and structure*, Vol. 6 (Ed: J. R. Durig), Elsevier, Amsterdam **1977**, p. 1.
[13] D. Papoušek, M. R. Aliev, *Molecular Vibrational-rotational Spectra: Theory and Applications of High Resolution Infrared, Microwave and Raman Spectroscopy of Polyatomic Molecules*, Elsevier Science Ltd, Amsterdam-Oxford-New York **1982**.
[14] M. D. Allendorf, C. F. Melius, *J. Phys. Chem. A* **1997**, *101*(14), 2670.
[15] O. Christiansen, *Phys. Chem. Chem. Phys.* **2012**, *14*, 6672.
[16] D. Oschetzki, G. Rauhut, *Phys. Chem. Chem. Phys.* **2014**, *16*, 16426.
[17] D. A. Clabo, W. D. Allen, R. B. Remington, Y. Yamaguchi, H. F. Schaefer, *Chem. Phys.* **1988**, *123*, 187.
[18] M. Piccardo, J. Bloino, V. Barone, *Int. J. Quantum Chem.* **2015**, *115*(15), 948.
[19] R. Ramakrishnan, G. Rauhut, *J. Chem. Phys.* **2015**, *142*, 154118.
[20] K. M. Christoffel, J. M. Bowman, *Chem. Phys. Lett.* **1982**, *85*, 220.
[21] J. M. Bowman, K. Christoffel, F. Tobin, *J. Phys. Chem.* **1979**, *83*, 905.
[22] T. Mathea, T. Petrenko, G. Rauhut, *J. Comput. Chem.* **2022**, *43*, 6.
[23] T. Mathea, G. Rauhut, *J. Comput. Chem.* **2021**, *42*, 2321.
[24] O. Christiansen, *J. Chem. Phys.* **2004**, *120*, 2149.
[25] P. Seidler, O. Christiansen, *J. Chem. Phys.* **2007**, *126*, 204101.
[26] K. Yagi, S. Hirata, K. Hirao, *Theor. Chem. Accounts* **2007**, *118*, 681.
[27] S. Erfort, M. Tschöpe, G. Rauhut, *J. Chem. Phys.* **2020**, *152*(24), 244104.
[28] S. Erfort, M. Tschöpe, G. Rauhut, *J. Chem. Phys.* **2022**, *156*, 124102.
[29] H. J. Werner, P. Knowles, F. Manby, et al., *J. Chem. Phys.* **2020**, *152*, 144107.
[30] T. B. Adler, G. Knizia, H. J. Werner, *J. Chem. Phys.* **2007**, *127*, 221106.
[31] F. Weigend, A. Köhn, C. Hättig, *J. Chem. Phys.* **2002**, *116*, 3175.
[32] S. Carter, S. J. Culik, J. M. Bowman, *J. Chem. Phys.* **1997**, *107*(24), 10458.
[33] J. M. Bowman, T. Carrington Jr., H. D. Meyer, *Mol. Phys.* **2008**, *106*, 2145.
[34] K. Pflüger, M. Paulus, S. Jagiella, T. Burkert, G. Rauhut, *Theor. Chem. Accounts* **2005**, *114*, 327.
[35] D. Kats, F. R. Manby, *J. Chem. Phys.* **2013**, *139*, 021102.
[36] D. Kats, D. Kreplin, H. J. Werner, F. R. Manby, *J. Chem. Phys.* **2015**, *142*, 064111.
[37] B. Ziegler, G. Rauhut, *J. Chem. Phys.* **2018**, *149*, 164110.
[38] B. Ziegler, G. Rauhut, *J. Chem. Phys.* **2016**, *144*, 114114.
[39] K. A. Peterson, T. B. Adler, H. J. Werner, *J. Chem. Phys.* **2008**, *128*(8), 084102.
[40] H. J. Werner, G. Knizia, F. R. Manby, *Mol. Phys.* **2011**, *109*(3), 407.
[41] M. Neff, G. Rauhut, *J. Chem. Phys.* **2009**, *131*, 124129.
[42] J. K. Watson, *Mol. Phys.* **1968**, *15*(5), 479.
[43] V. Špirko, P. Jensen, P. Bunker, A. Čejchan, *J. Mol. Spectrosc.* **1985**, *112*(1), 183.
[44] S. N. Yurchenko, A. Yachmenev, R. I. Ovsyannikov, *J. Chem. Theory Comput.* **2017**, *13*(9), 4368.
[45] P. Bunker, P. Jensen, *Molecular Symmetry and Spectroscopy*, 2nd ed., NRC Research Press, Ottawa, ON, Canada **1998**.
[46] T. A. Ruden, T. Helgaker, P. Jørgensen, J. Olsen, *J. Chem. Phys.* **2004**, *121*, 5874.
[47] J. Koput, K. A. Peterson, *J. Chem. Phys.* **2006**, *125*, 044306.
[48] P. Meier, M. Neff, G. Rauhut, *J. Chem. Theory Comput.* **2011**, *7*, 148.
[49] H. Allen, P. Cross, *Molecular Vib-Rotors: The Theory and Interpretation of High Resolution Infrared Spectra*. LCCN, John Wiley and Sons, Inc., New York and London **1963**, p. 63.

SUPPORTING INFORMATION

Additional supporting information may be found in the online version of the article at the publisher's website.

How to cite this article: M. Schneider, G. Rauhut, *J. Comput. Chem.* **2023**, *44*(3), 298. https://doi.org/10.1002/jcc.26893